Micellization of an asymmetric block copolymer in mixed selective solvents

Chikako Honda* and Keiko Sakaki
Showa College of Pharmaceutical Sciences, Higashitamagawa-gakuen 3-3165, Machida-shi, Tokyo 194, Japan

and Takuhei Nose
Department of Polymer Chemistry, Tokyo Institute of Technology, Ookayama, Meguro-ku, Tokyo 152, Japan
(Received 11 January 1994; revised 7 April 1994)

Micelle formation and decomposition were investigated by static and dynamic light scattering for the diblock copolymer poly(α-methylstyrene)-*block*-poly(vinyl-*p*-phenethyl alcohol) (PαMS-*b*-PVPA) with asymmetric block composition [PαMS]/[PVPA] = 90/10 (in molar mass) in mixed solvents, one component solvent, *m*-chlorobenzyl chloride (CBC), being selective for the PαMS block and the other, *m*-chlorobenzyl alcohol (CBA), being so for the PVPA block. Core–corona type micelles were formed in both pure solvents: micelles in CBA were dense star-shaped 'crew-cut' ones having a large swollen core with a thin corona layer, and those in CBC were star-shaped ones having a small core with long corona chains. Micelle decomposition was observed in both CBA- and CBC-rich solvents within a narrow range of solvent composition as the other component solvent was being added to a pure solvent. In the case of micelles formed in CBA-rich solvents, micellization could be induced by decreasing the temperature, while the micelles in CBC-rich solvents could not be decomposed in the ordinary temperature range. The temperature-induced micellization transition at higher polymer concentrations took place with no appreciable increase of micelle fraction but primarily with an increase of association number. On the other hand, in the transition region at a lower concentration, change of micelle fraction dominated over variation of association number. From these results, the following were suggested: the critical micelle concentration *cmc** near the critical micelle temperature was located at a relatively high concentration in CBA-rich solvents, while the micelles formed in CBC-rich solvents were more stable having lower *cmc**.

(Keywords: block copolymer; micellization; light scattering)

INTRODUCTION

Micellization of diblock copolymers in selective solvents has been studied extensively from both theoretical[1–11] and experimental[12–29] viewpoints. Micelle structures and conditions of their formation have been studied experimentally as functions of chain lengths of total block copolymers and constitutional blocks, composition of mixed solvent, polymer concentration and temperature by using static and dynamic light scattering[12–21] and other experimental techniques such as small-angle X-ray scattering[22,23], neutron scattering[24], nuclear magnetic resonance[25] and gel permeation chromatography[26].

Micelle formation is essentially closed association, having a critical micelle concentration (*cmc*) that is usually very dilute. Because of the low *cmc*, it is not very easy under ordinary conditions to observe *cmc* for studying the process and/or conditions of micelle formation. Using dynamic light scattering, Zhou *et al.*[21] evaluated concentrations of unimers and micelles near the critical micelle temperature for temperature-induced micelle formation of polystyrene-*block*-poly(t-butylstyrene) in *N*,*N*-dimethylacetamide. Malmstem *et al.*[28] applied gel permeation chromatography and self-diffusion measurements to aqueous solutions of poly(ethylene oxide)-*block*-poly(propylene oxide)-*block*-poly(ethylene oxide) and found that decrease of *cmc* and increase in association number and micelle size with increasing temperature were consistent with the predictions of a self-consistent lattice theory for a multicomponent system of copolymers. Tsunashima[18] observed the *cmc* at a very dilute polymer concentration, i.e. of the order of 1×10^{-4} g ml^{-1}, for polystyrene-*block*-polybutadiene in n-decalin using dynamic light scattering.

This study aims to investigate micelle formation and decomposition by measuring apparent molecular weight and apparent radius of gyration as functions of thermodynamic conditions using light scattering. Particular attention has been paid to change of association number and fraction of micelle-forming polymers near the transition between unimers and micelles.

To achieve this aim, we used mixed solvents, each of the pure solvents being selective for each of the blocks of the copolymer. Favourable requirements for the solvents are that they are well miscible and isorefractive with each other, and isorefractive with one block, too. Change in the composition of these solvents can make the solvent quality (solvent selectivity) of the mixed

* To whom correspondence should be addressed

0032-3861/94/24/5309–10

solvent change continuously with no problem of refractive-index change of solvent in light scattering measurements. No strong preferential adsorption of solvent may be expected because of the good miscibility of the solvents. By means of this technique, we can easily find conditions for observing the transition of micelle formation and decomposition at an appropriate polymer concentration and temperature, and also we can see the asymmetry effects, i.e. effects of difference in chain length between core and corona, if any, using a single block copolymer with very different block sizes, because blocks forming core and corona reverse in one pure solvent with respect to the other pure solvent.

We selected poly(α-methylstyrene)-*block*-poly(vinyl-*p*-phenethyl alcohol) with a very asymmetric block composition, and *m*-chlorobenzyl chloride/*m*-chlorobenzyl alcohol as mixed solvent. Static and dynamic light scattering measurements have been carried out on their dilute solutions as functions of solvent composition, temperature and polymer concentration. Based on the results, we discuss the micelle structure with association number, and the behaviour of their formation and decomposition.

EXPERIMENTAL

Materials

Poly(α-methylstyrene)-*block*-poly(vinyl-*p*-phenethyl alcohol) (PαMS-*b*-PVPA) was an anionically polymerized product with the sample code KT-327[30], and the number-average molecular weights of the PαMS and PVPA blocks were 1.13×10^5 g mol^{-1} and 1.24×10^4 g mol^{-1}, respectively. Molecular-weight distribution index M_w/M_n was around 1.1.

The purchased solvents *m*-chlorobenzyl chloride (CBC) and *m*-chlorobenzyl alcohol (CBA) were purified by distillation before use. Refractive indices of CBC and CBA after purification were 1.5526 and 1.5522 for D-line light at 25°C, respectively, being almost identical with each other.

Light-scattering measurement

Static and dynamic light scattering were carried out by using a DLS-700 apparatus (Ohtsuka Electronic Co. Ltd), with an Ar-ion laser operated at 488 nm as light source.

Solvents were optically purified by Teflon filter with nominal pore size of 0.2 μm. Stock solutions were prepared by dissolving the block polymers in the solvents and keeping the solutions at 50–55°C for 2–3 h, and were optically purified by Teflon filter with nominal pore size of 0.45–0.65 μm. The stock solution was diluted by adding the purified solvent in a dust-free optical cell to make a sample solution with the desired concentration ranging from 0.4×10^{-4} to 1×10^{-3} g/(g solution). Subsequently, the optical cell was flame sealed under mild vacuum, and was left at 40°C for four days for the sake of stabilization of the solution before light scattering measurements.

Excess Rayleigh ratio $\Delta R(\theta)$ was calculated from the measured excess scattered intensity using the intensity of benzene as standard, with the Rayleigh ratio of benzene being 3.405×10^{-5} cm^{-1} at 25°C[31]. The measured excess Rayleigh ratio as a function of scattering angle θ and concentration C (g ml^{-1}) was described by:

$$\frac{KC}{\Delta R(\theta)} = \frac{1}{M_w}\left[1 + \frac{16\pi^2 n^2}{3\lambda_0^2} R_g^2 \sin^2\left(\frac{\theta}{2}\right)\right] + 2A_2C + \cdots \quad (1)$$

where M_w, R_g^2 and A_2 are weight-average molecular weight, z-average mean square radius of gyration and second virial coefficient, respectively, and K is the optical constant defined by:

$$K = 4\pi^2 n^2 (dn/dC)^2/\lambda^4 N_A$$

with n, λ_0 and N_A being the refractive index, the wavelength of the incident beam and the Avogadro constant, respectively. The refractive-index increment (dn/dC) for the CBC solution of the block copolymer was measured by a differential refractometer (DRM-1020, of Ohtsuka Electronic Co. Ltd) to be 0.065 ml g^{-1} for $\lambda_0 = 488$ nm at 30°C, which was used for the solutions of solvents CBC, CBA and their mixtures, because CBC and CBA are virtually isorefractive. M_w, R_g^2 and A_2 were determined by a Zimm plot. Since the measured (dn/dC) for PVPA in CBA, being 0.0048 ml g^{-1}, was very small compared with that of the copolymer solution, the obtained R_g^2 can be regarded as the R_g^2 of the PαMS part of a micelle.

In some mixed solvents where formation and decomposition of micelles were observed, the above conventional analysis could not be available because extrapolation to the dilute limit was not allowed since the structure and/or the fraction of micelles could change with concentration. In this case, without the extrapolation, we evaluated apparent molecular weight $M_{w,app}$ and apparent radius of gyration $R_{g,app}$, which were defined as:

$$M_{w,app} = \frac{\Delta R(0)}{KC} \quad (2)$$

$$R_{g,app}^2 = \frac{(\text{initial slope})3\lambda_0^2 M_{w,app}}{16\pi^2 n^2} \quad (3)$$

$KC/\Delta R(0)$ and (initial slope) are the intercept and the initial slope of the Zimm plot, $KC/\Delta R(\theta)$ vs. $\sin^2(\theta/2)$, at finite concentrations.

The autocorrelation function $g^{(2)}(\tau)$ of the scattered intensity was transformed to the correlation function $g^{(1)}(\tau)$ of the electric field of the scattered light by the following equation of the self-beat method:

$$g^{(2)}(\tau) = A[1 + B|g^{(1)}(\tau)|^2] \quad (4)$$

where A and B are constants. The correlation function $g^{(1)}(\tau)$ of the electric field of the scattered light was analysed by the cumulant method[32], i.e. from the non-linear least-squares fitting to the cumulant expansion:

$$|g^{(1)}(\tau)| = \exp(-\bar{\Gamma}\tau + \tfrac{1}{2}\mu_2\tau^2 - \cdots) \quad (5)$$

We evaluated the average decay rate $\bar{\Gamma}$ and the second cumulant μ_2. The obtained value of $\mu_2/\bar{\Gamma}^2$ ranged from 0.003 to 0.1, showing that the decay of $g^{(1)}(\tau)$ was almost single-exponential decay, so that the particle size distribution was reasonably narrow in most cases. The decay rate $\bar{\Gamma}$ obtained for any solvents followed the q^2 dependence, i.e. $\bar{\Gamma} = Dq^2$, where q is the length of the scattering vector defined as $q = (4\pi n/\lambda_0)\sin(\theta/2)$. The diffusion coefficient D calculated from $\bar{\Gamma}$ as a function of concentration C was extrapolated to infinite dilution to

obtain the diffusion coefficient D_0 at $C = 0$. The hydrodynamic radius R_h was calculated with the Stokes–Einstein equation:

$$R_h = \frac{k_B T}{6\pi\eta D_0} \quad (6)$$

where k_B, T and η are the Boltzmann constant, absolute temperature and solvent viscosity. The viscosity η was measured by an Ubbelohde-type viscometer as a function of temperature and the composition of CBC and CBA. Similarly to the static properties, in the transition region of micellar formation and decomposition, extrapolation to zero concentration could not be done, so we evaluated the hydrodynamic radius without extrapolation, which was referred to as the apparent hydrodynamic radius, $R_{h,app}$.

RESULTS AND DISCUSSION

Micelles in pure CBC

The static and dynamic properties of micelles formed in CBC at 30°C are summarized in *Tables 1* and *2*. Since the PVPA block, which is the shorter block of the present block copolymer, should form the core part of a micelle in the relatively hydrophilic solvent CBC, the micelle in CBC must be of a star-like structure with a small centre core and about 97 arm chains as depicted in *Figure 1*.

The estimated structure was confirmed by comparing measured R_g and R_h with those of real star-shaped polymers.

Assuming the star shape for the micelle, R_g was estimated from the fact that the ratio $g_{ga} \equiv R_g(\text{star})/R_g(\text{arm})$ of the radius of gyration, R_g(star), of a star polymer to that, R_g(arm), of the arm in a good solvent depends on the number f of arms only[33–38]. The radius of the PαMS block, which corresponds to R_g(arm) in the present case, was calculated from the relation $R_g = 1.485 \times 10^{-9} M^{0.577}$ in the good solvent, toluene[39], to be 12.2 nm. The estimated value of R_g(star) was 42.3 nm from the modified Flory theory $g_{ga} = 1.39 f^{1/5}$ (ref. 36), 35.1 nm from the experimental relation $g_{ga} = 1.48 f^{0.145}$ (for $f < 22$) by Okada *et al.*[38], and 43.9 nm from the experimental equation $g_{ga} = g_g^{1/2} f^{\nu} = (1.67)^{1/2} f^{\nu - 0.364}$ (for $4 \leqslant f \leqslant 269$) with $\nu = 0.588$ by Roovers *et al.*[37]. Here, $g_g = R_g^2(\text{star})/R_g^2(\text{linear})$. The measured value of R_g, 46.1 nm, is a little larger than these values, but is closer to the values estimated from the equations for larger f, and supports the star-shaped micelle if one notices the presence of the core with a finite size in the micelle. The ratio ρ of R_g to the hydrodynamic radius R_h, $\rho = R_g/R_h$, is 0.77 as shown in *Table 2*, being consistent with those reported for star-shaped particles, i.e. $\rho = 0.75$ to 0.82 for star-shaped polybutadienes with $f > 200$[38], and $\rho = 0.75$ for a micelle of poly(ethylene oxide)-*block*-polystyrene with $f = 100$ in cyclopentane[40].

Figure 1 Schematic representation of estimated micelle structure formed in CBC

Table 1 Static properties of KT-327 micelles at 30°C

Solvent	$M_w \times 10^7$ (g mol^{-1})	R_g (nm)	A_2 (cm^3 mol g^{-2})
CBA	3.27	21.6	5.16×10^{-6}
CBC	1.21	46.1	1.27×10^{-5}

Table 2 Dynamic properties of KT-327 micelles at 30°C

Solvent	$D_0 \times 10^8$ (cm^2 s^{-1})	R_h (nm)	μ_2/Γ^2	R_g/R_h
CBA	0.736	39.4	0.0397	0.548
CBC	2.17	59.9	0.0859	0.770

Micelles in pure CBA

The static and dynamic properties of micelles formed in CBA at 30°C are summarized in *Tables 1* and *2*. Since the PS block, which is the longer block of the present block copolymer, should form the core part of a micelle in the relatively hydrophilic solvent CBA, the micelle in CBA must be of a 'crew-cut' structure, i.e. a large core with a thin corona layer as depicted in *Figure 2*. Since the solvent is substantially isorefractive with the corona of PVPA, the measured R_g is the radius of gyration of the core, while R_h is the radius of the whole micelle including the corona. If the core were not swollen with the solvent, the radius of gyration would have to be 17.5 nm, which is much smaller than the measured value of 21.6 nm. Here, R_g was estimated from $R_g = (3/5)^{1/2} R$ with the radius R of the core, which was calculated from the molar mass (3.27×10^7 g mol^{-1}) of PαMS core in the micelle and the density of bulk PαMS (1.1296 g cm^{-3}) at 30°C[41], assuming the isorefractivity for the PVPA corona (see Appendix 1). This means that the core part must swell with the solvent. Taking this fact into account, one can suppose a few possible structures of the associate, including vesicle. To judge the most provable structure of the obtained associate, we calculated the segment density profile for three spherical models that reproduce the measured values of R_g and R_h. The three models are (a) a core–corona with uniform segment density, (b) a core–corona with segment-density gradient, and (c) a vesicle, which are illustrated in *Figure 2*. Details of the calculation are described in Appendix 1. The vesicle structure looked to be a possible structure that was compatible with the large core, but in reality is most unlikely, judging from the observed ratio of R_g/R_h. The vesicle structure should generally give a value of R_g/R_h close to unity because R_g must be close to the radius of the shell, which is close to R_h. As a consequence of this, the calculated structure that reproduces the observed R_g has a very small radius R of PαMS shell, and the distance between the R of PαMS and the outer radius of the vesicle seems too large to be made up by the PVPA chains. The unperturbed end-to-end distance and the fully extended length of the PVPA-block chain were calculated to be

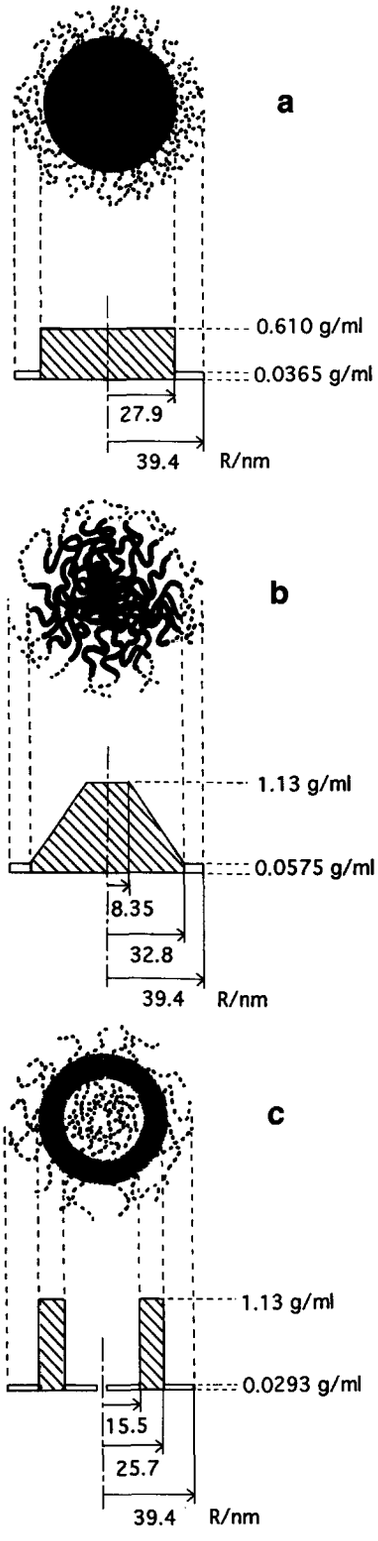

Figure 2 Schematic representations of estimated micelle structures formed in CBA: (a) a core–corona with uniform segment density; (b) a core–corona with segment-density gradient; and (c) a vesicle. The structure (b) is most likely

6.9 nm and 20.9 nm, respectively, while the calculated thickness of PVPA corona layer was 13.7 nm. Here, the characteristic segment length $L_0/N^{0.5}$, with L_0 and N being the unperturbed end-to-end distance and degree of polymerization, respectively, was put to be 0.757 nm, which was common for PαMS[39], polystyrene[42] and poly(*p*-methylstyrene)[43] within experimental accuracy. For the fully extended chain, a planar zig-zag with the length of monomer unit being 2.52 Å was assumed for the extended chain.

In the case of (a), the radius of the core should be 27.9 nm, leading to the concentration of PαMS in the core being 53.2 vol% and the thickness of PVPA corona layer being 11.5 nm. Considering the chain dimension of the PVPA block (see above), the obtained corona thickness seemed too large. Furthermore, it looks unlikely that the PαMS block chain, which has end-to-end distance of 30 nm in a good solvent[39], had to be greatly extended as much as it is in dilute solution and swollen in the core to have a 'uniform' concentration of 53.2 vol%. The most realistic structure may be the case (b), where the segment density changes gradually and continuously at the interface between the core and the corona. The core chain segment near the interface must be much more swollen than that in the inside of the core by the excluded-volume effects of the corona PVPA block. In reality the interface between the core and the corona may be diffuse, although the model assumed a sharp interface. In conclusion, the estimated structure is a 'dense' star-shaped 'crew-cut' (b) rather than the discrete two-phase core–corona structure.

Transition of micelle formation and decomposition induced by temperature and solvent composition

Figure 3 shows the change of apparent association number P_{app} with composition of the mixed solvent for the polymer concentration $C = 3.14 \times 10^{-4}$ g/(g solution) at 30°C, where P_{app} was given by M_{app}/M_{uni}, with M_{uni} being M_w of the block copolymer. In CBA-rich solvents, the apparent association number sharply decreased with increasing CBC content in the composition range [CBC]/[CBA] = 0.1/0.9 to 0.18/0.82, and no micelle formation could be detected at [CBC]/[CBA] = 0.2/0.8, where [X] is the concentration of X in weight. On the other hand, in CBC-rich solvents, the apparent association number showed a relatively gradual

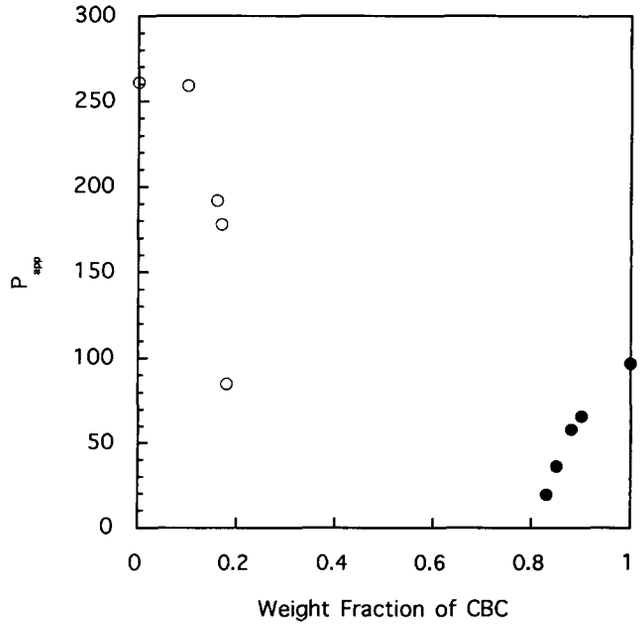

Figure 3 Dependence of apparent association number, P_{app}, on solvent composition at 30°C. Polymer concentration is 3.14×10^{-4} g/(g solution)

decrease with increasing CBA content, and no association was detected at [CBC]/[CBA] = 0.8/0.2.

The sharp formation and decomposition of micelles in CBA-rich solvents could also be induced by temperature change. *Figure 4* shows the temperature dependence of apparent molecular weight M_{app} and apparent radius of gyration $R_{g,app}$ for the micelles formed at the block-copolymer concentration of 3.14×10^{-4} g/(g solution) in CBA-rich mixed solvents under cooling at a rate of 1°C/30 min after decomposing the micelles at 50°C for [CBC]/[CBA] = 0.1/0.9, or at 40°C for other solvent compositions. One can notice that M_{app} and $R_{g,app}$ changed in parallel very rapidly in a narrow temperature range. This parallel change of M_{app} and $R_{g,app}$ implies that micelle formation and decomposition took place without appreciable change in the fraction θ of micelle-forming block copolymers, but primarily with changing the association number P. Otherwise, $R_{g,app}$ would have to be almost independent of M_{app}. Here, one should recall that M_{app} is the weight-average molecular weight while $R_{g,app}$ is the z-average radius of gyration. Accordingly, M_{app} is approximately the product of the molecular weight of micelles and the fraction θ in weight, whereas $R_{g,app}$ is close to the true radius of gyration R_g of micelles, and insensitive to θ because of the large molecular weight of micelles compared with that of unimers. The parallel change of M_{app} and $R_{g,app}$ is illustrated more quantitatively in *Figure 5*, where $R_{g,app}$ changing with temperature was plotted against M_{app} for different solvent compositions in log–log scale. $R_{g,app}$ monotonically decreases with decreasing M_{app}. All data points fall approximately on a single master curve irrespective of temperature and the solvent composition, although the plots depend on the solvent composition at lower M_{app}, i.e. at higher temperatures. The master curve at higher M_{app} where the micelles have grown well is described by a power law $R_{g,app} \propto M_{app}^{\nu}$ with $\nu = 0.26$. The exponent is smaller than that for a rigid sphere, 1/3. This fact may come partly from the change of the micelle-forming fraction θ and partly from the micelle

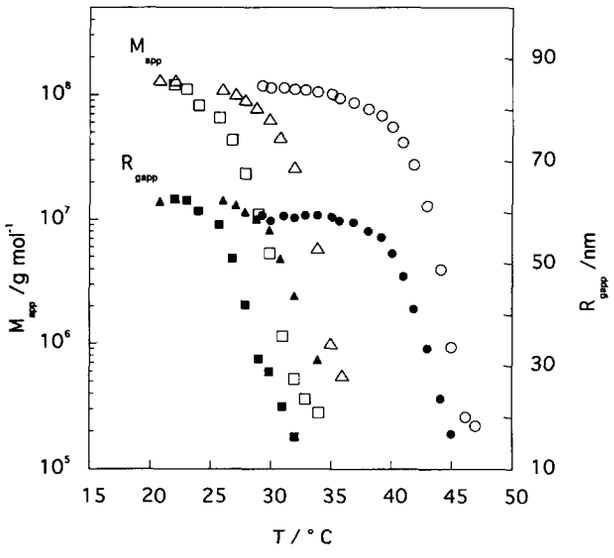

Figure 4 Temperature dependence of M_{app} and $R_{g,app}$ at the fixed block-copolymer concentration of 3.14×10^{-4} g/(g solution) for various solvent compositions. M_{app}: CBC weight fraction = 0.1 (○), 0.16 (△) and 0.18 (□). $R_{g,app}$: CBC weight fraction = 0.1 (●), 0.16 (▲) and 0.18 (■)

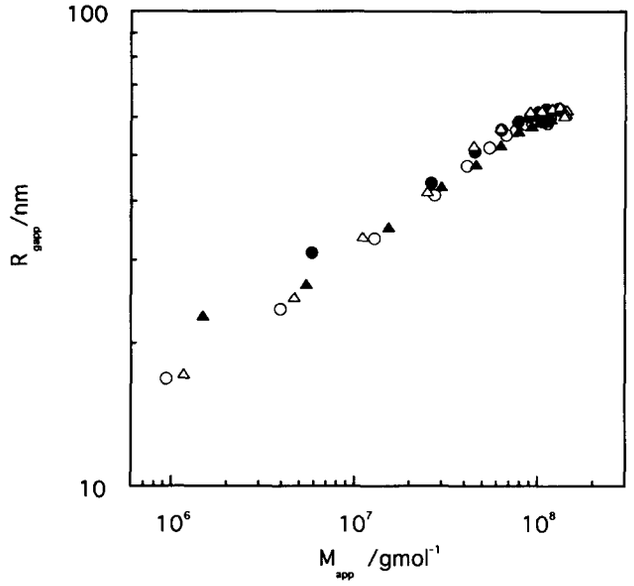

Figure 5 Relationship between $R_{g,app}$ and M_{app} with changing temperature at the polymer concentration of 3.14×10^{-4} g/(g solution) in CBA-rich mixed solvents. Solvent composition: CBC weight fraction = 0.1 (○), 0.16 (●), 0.17 (△) and 0.18 (▲)

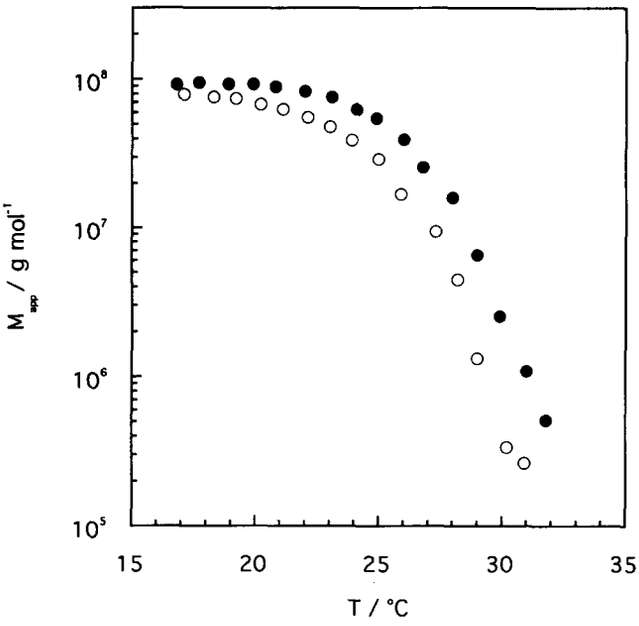

Figure 6 Temperature dependence of M_{app} under cooling (○) and then heating (●) at a rate of 1°C/30 min. It took about 6 min to measure a set of data of angular dependence of scattered-light intensity

structure. The fraction θ may be close to unity but decrease slightly with increasing temperature, which results in the smaller exponent because M_{app} is smaller than the true molecular weight M_w by the factor θ. The estimated structure is not a rigid sphere but a dense star shape, which may have a lower M_w dependence of R_g than that of a rigid sphere since the exponent of arm number (f) dependence for molecular weight of star-shaped polymers is less than 1/3, being 0.236 for dense star-shaped polymers with large f (see the previous section)[38].

Figure 6 represents the reversibility of the transition of micelle formation and decomposition, where M_{app} were

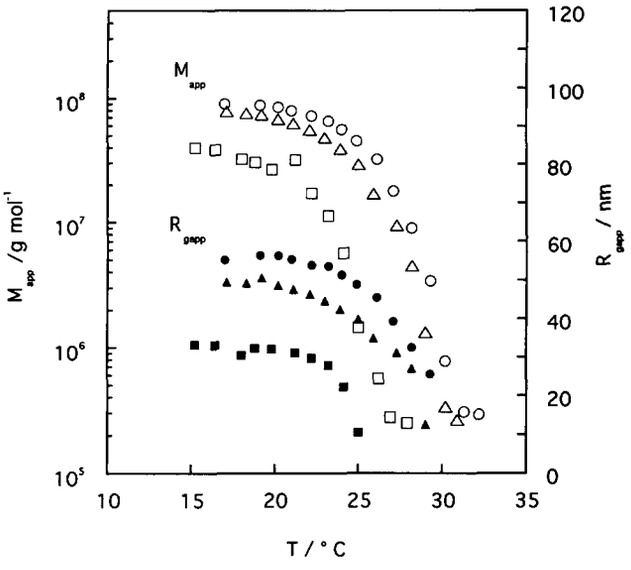

Figure 7 Temperature dependence of M_{app} and $R_{g,app}$ for various polymer concentrations in the mixed solvent (CBC weight fraction = 0.18). M_{app}: polymer concentration = 4.66×10^{-4} (○), 3.21×10^{-4} (△) and 1.52×10^{-4} g/(g solution) (□). $R_{g,app}$: polymer concentration = 4.66×10^{-4} (●), 3.21×10^{-4} (▲) and 1.52×10^{-4} g/(g solution) (■)

plotted against temperature T observed under cooling and heating at a rate of 1°C/30 min for the solution of $C = 3.21 \times 10^{-4}$ g/(g solution) and [CBC]/[CBA] = 0.18/0.82. The micelles formed in heating and cooling processes have different M_{app} at the same temperature, which obviously shows that the observed behaviour of the transition is not an equilibrium one, but somewhat includes kinetic effects. Details on the kinetics of micelle formation and decomposition will be discussed elsewhere.

Figure 7 represents the polymer-concentration dependence of M_{app} vs. T and $R_{g,app}$ vs. T relations at the solvent composition [CBC]/[CBA] = 0.18/0.82. The relation between M_{app} and $R_{g,app}$ is represented in *Figure 8*.* Parallel variation of M_{app} and $R_{g,app}$ is found at higher concentrations, approximately making the master curve with other data shown in *Figure 5*, showing no essential change in micelle structure and micelle-forming fraction with concentration. On the other hand, the change of $R_{g,app}$ with M_{app} at lower concentration is different from that at higher concentrations. Namely, at a concentration of 1.52×10^{-4} g/(g solution), $R_{g,app}$ shows a very slight decrease with decreasing M_{app} at higher M_{app}, which strongly suggests that change of micelle-forming fraction dominates over that of association number in this temperature-induced micellization, in contrast to the case of higher concentrations. It can also be pointed out that $R_{g,app}$ at large M_{app} is appreciably smaller than those of higher concentrations compared at the same M_{app}. This fact may suggest an essential difference in micelle structure between lower and higher concentrations. The presence of a structural transition with changing concentration cannot definitely be concluded here, and may not theoretically be expected in general. However, actually Tsunashima[18] has observed a structural transition with change of polymer concentration by dynamic light scattering.

In contrast to the micelles in CBA-rich mixed solvents, the star-shaped micelles formed in CBC-rich mixed solvents exhibited no essential change of their structure and fraction θ with polymer concentration and temperature. No sign of disassociation with increasing temperature was found up to 60°C in the solvent composition range of [CBC]/[CBA] = 1/0 to 0.83/0.13. The concentration dependence of the integrated intensity of scattered light as a function of scattering angle could be analysed by a Zimm plot for micellar solutions of [CBC]/[CBA] = 0.83/0.17 with $C = 2.48 \times 10^{-4}$ to 7.87×10^{-4} g/(g solution). (In CBA-rich mixed solvents, the A_2 effects (i.e. finite-concentration effects) on the discrepancy of M_{app} and $R_{g,app}$ from the real M_w and R_g are negligible compared with their change with temperature and concentration discussed here.) M_w, A_2 and R_g obtained from the Zimm plots as a function of temperature are listed in *Table 3*. It is noted that M_w increases slightly with increasing temperature, accompanying an increment of A_2 and no change of R_g. A possible explanation for the increase of M_{app} is that solvent quality for the core becomes poorer because of

Table 3 Characteristics of micelles formed in the CBC-rich mixed solvent of [CBC]/[CBA] = 0.83/0.17 in weight at various temperatures

Temperature (°C)	$M_w \times 10^6$ (g mol^{-1})	R_g (nm)	$A_2 \times 10^4$ (cm^3 mol g^{-2})
46	7.143	46.3	2.675
40	6.452	46.9	1.958
32	4.862	46.3	0.876
24	4.738	47.7	0.763

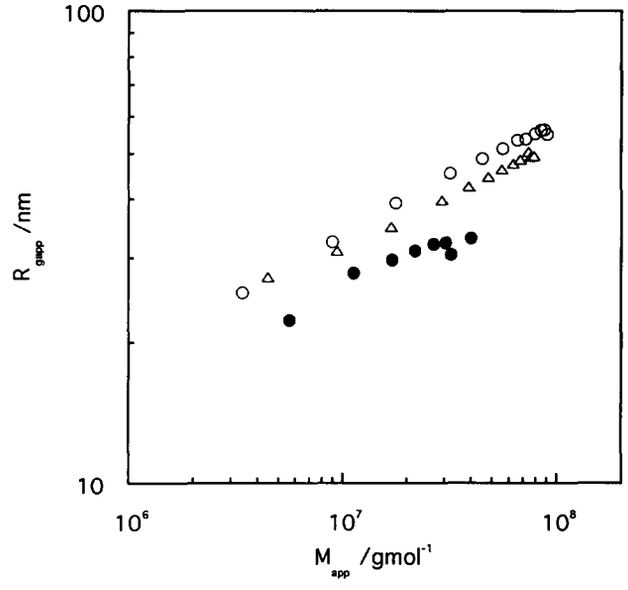

Figure 8 Relationship between $R_{g,app}$ and M_{app} with changing temperature in CBA-rich mixed solvent (CBC weight fraction = 0.18) for various polymer concentrations: 4.66×10^{-4} (○), 3.21×10^{-4} (△) and 1.52×10^{-4} g/(g solution) (●)

*Solutions with nearly equal polymer concentration, which were prepared at different times, could have different micelle sizes, as in the case of solutions of 3.14×10^{-4} g/(g solution) in *Figure 4* and 3.21×10^{-4} g/(g solution) in *Figure 7*. Even in such a case, the micelle-forming temperature was independent of solution preparation, and the relationships between M_{app} and $R_{g,app}$ in the micelle-forming process, characterized by the log–log plots of M_{app} and $R_{g,app}$, for the independently prepared solutions, were consistent with each other

reduction of the hydrogen-bonding effect of added CBA with increasing temperature. One may attribute this temperature dependence of M_{app} to other facts, e.g. to kinetic effects or to a sign of the anomalous micellization observed near the critical micelle-forming temperature[16,43,45]. It is difficult, however, to reach a definite conclusion, because there remains uncertainty in the extrapolation to zero concentration in determining M_w, A_2 and R_g, especially A_2, since we assumed no change of the micelle structure with concentration.

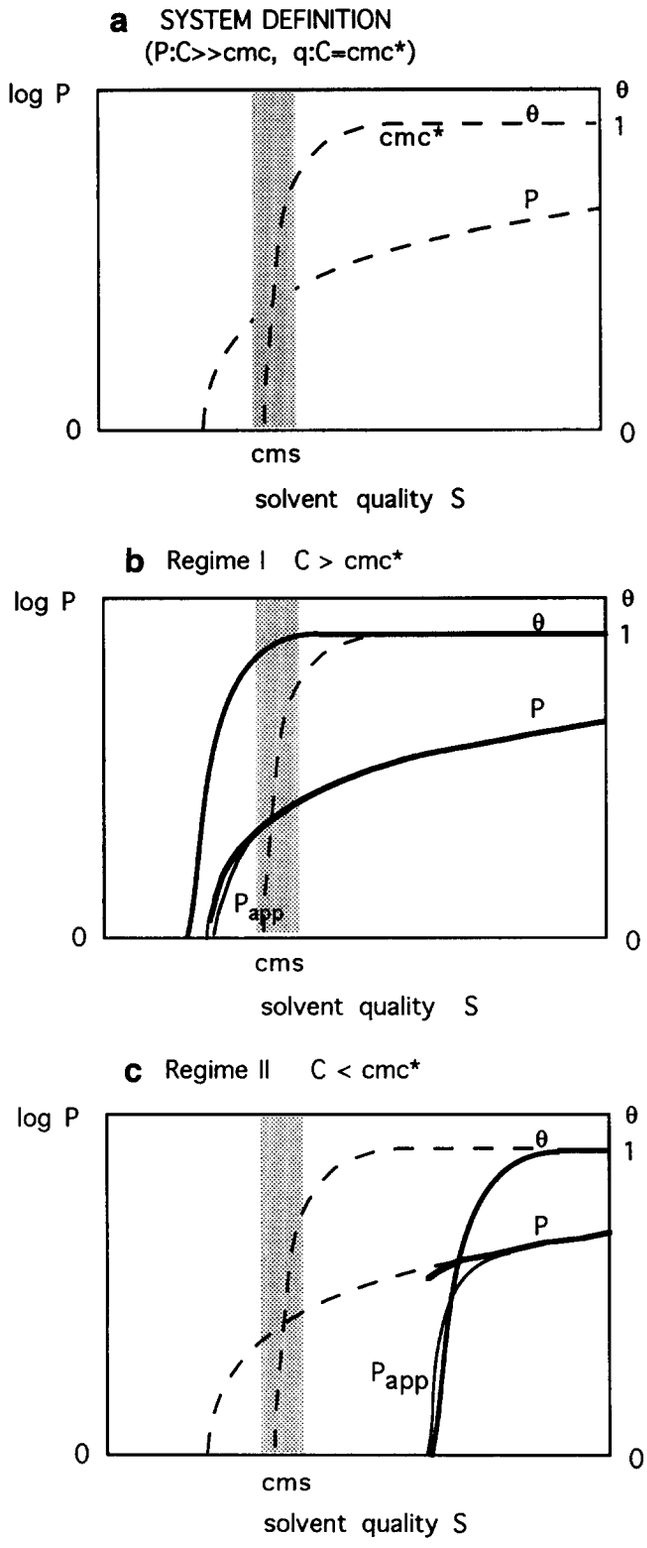

Figure 9 Schematic representation of P and θ changes with solvent quality S; *cms* is the solvent quality of critical micelle, and *cmc** is *cmc* at *cms*. (a) P for $C \gg cmc$ and θ for $C = cmc^*$; (b) regime I ($C > cmc^*$); and (c) regime II ($C < cmc^*$)

Expected changes of the association number P and the micelle-forming fraction θ with solvent quality S at different polymer concentrations C are illustrated schematically in *Figure 9*, which is based on calculations with the Leibler–Orland–Wheeler (LOW) theory[2,7]. Details of the calculation are described in Appendix 2. The solvent quality S is defined such that it has a larger value for the stronger segregation of block copolymers to form micelles in a selective solvent, which is evaluated by the effective interfacial free energy at the core surface. In the present case, the value of S varies with temperature and solvent composition. The association number P is primarily determined by S only, being almost independent of C as long as $C > cmc$. The fraction θ as a function of S depends on C, in other words, *cmc* depends on S, i.e. the θ–S curve shifts to the higher S side when C becomes lower. Critical micelle solvent quality *cms* is defined as S at the onset of micelle decomposition (or formation) at $C \gg cmc$, and *cmc** is defined as *cmc* at *cms* (see *Figure 9*). Then, we can suppose two regimes defined by C relative to *cmc**, which exhibit different characteristic P and θ changes at the transition of micelle forming and decomposition, as shown in *Figure 9*. In regime I of $C > cmc^*$, the transition takes place with P change near *cms*, where the fraction θ is almost levelled off, reaching unity, with no appreciable change with S and C. On the contrary, in regime II of $C < cmc^*$, the transition takes place with θ change around a certain S, which is larger than *cms* and depends on C, where P shows a mild change with S. Consequently, in regime I, both $R_{g,app}$ and M_{app} change in parallel with solvent quality, but show no large variation with concentration. On the other hand, in regime II, M_{app} changes quickly with solvent quality owing to θ change, while the $R_{g,app}$ change is not so large because of a mild P change compared with M_{app} change. It should be recalled here that $R_{g,app}$ reflects P, while M_{app} is proportional to $P\theta$.

In CBA-rich solvents, no appreciable changes of P and θ with C were found, while P changed with temperature, at higher concentrations. It follows that this experimental region is considered to be in regime I ($C > cmc^*$), although the slight increases of M_{app} and R_{app} with C (*Figure 7*) suggest that the concentration region is not so far away from *cmc**. The lower concentration may be located in regime II ($C < cmc^*$) since P change dominated over θ change. Zhou *et al.*[21] measured the hydrodynamic radius R_h of micelles formed by temperature-induced micellization and found no change of R_h, accordingly constant P, with temperature change near the critical micelle temperature. Their experimental range of concentration may be lower than *cmc**, being located in regime II.

In the CBC-rich solvents, no essential dependence of the micelle fraction θ on concentration was observed. This suggests that *cmc** in these solvents is lower than the experimental concentration (regime I). In the present experimental range of solvent composition, the association number P becomes smaller with increasing [CBA]/[CBC], but the micelles are still stable in the sense that $C \gg cmc^*$. If the [CBA] content in the solvent increases, the *cmc** will be higher and regime I could be observed. However, the association number would become so small and light scattering cannot easily

measure the structure of micelles because of low scattered intensity.

The above findings that C is around cmc^* for CBA-rich solvents, while $C \ll cmc^*$ for CBC-rich solvents, may be attributed to asymmetry of block chain lengths. The chain length N_0 of blocks forming the core is larger than corona-forming chain length N_1 in CBA-rich solvents, while $N_0 < N_1$ in CBC-rich solvents. Block copolymers with $N_0 > N_1$ easily form a large micelle with weak segregation of the core, where cmc^* can be relatively large. On the other hand, polymers with $N_0 < N_1$ need a strong segregation to form a micelle, usually with a relatively small association number. This results in a lower cmc^*. The theoretical calculations presented in Appendix 2 seem to support this speculation.

REFERENCES

1 Noolandi, J. and Hong, K. M. *Macromolecules* 1983, **16**, 1443
2 Leibler, L., Orland, H. and Wheeler, J. C. *J. Chem. Phys.* 1983, **79**, 3550
3 Whitmore, M. D. and Noolandi, J. *Macromolecules* 1985, **18**, 657
4 Roe, R.-J. *Macromolecules* 1986, **19**, 728
5 Halperin, A. *Macromolecules* 1987, **20**, 2943
6 Munch, M. R. and Gast, A. P. *Macromolecules* 1988, **21**, 1360
7 Marques, C., Joanny, J. F. and Leibler, L. *Macromolecules* 1988, **21**, 1051
8 Nagarajan, R. and Ganesh, K. *J. Chem. Phys.* 1989, **90**, 5843
9 Leibler, L. *Physica (A)* 1991, **172**, 258
10 Shim, D. F. K., Marques, C. and Cate, M. E. *Macromolecules* 1991, **24**, 5309
11 Yuan, X.-F., Masters, A. J. and Price, C. *Macromolecules* 1992, **25**, 6876
12 Tuzar, Z. and Kratochvil, P. *Adv. Colloid Interface Sci.* 1976, **6**, 201
13 Elis, H. G. in 'Light Scattering from Polymer Solutions' (Ed. M. B. Huglin), Academic Press, London, 1972, Ch. 9
14 Kotaka, T., Tanaka, T., Hattori, M. and Inagaki, H. *Macromolecules* 1978, **11**, 138
15 Zhou, Z. and Chu, B. *J. Interface Sci.* 1988, **126**, 171
16 Zhou, Z. and Chu, B. *Macromolecules* 1988, **21**, 2548
17 Tuzar, Z., Konak, C., Stepanec, P., Plestil, J., Kratochvil, P. and Prochazka, K. *Polymer* 1990, **31**, 2118
18 Tsunashima, Y. *Macromolecules* 1990, **23**, 2963
19 Tuzar, Z., Webber, S., Raniredd, C. and Munk, P. *Polym. Prepr.* 1991, **32**, 525
20 Xu, R., Winnik, M. A., Riuss, G., Chu, B. and Croucher, M. D. *Macromolecules* 1992, **25**, 644
21 Zhou, Z., Chu, B. and Peiffer, D. G. *Macromolecules* 1993, **26**, 1876
22 Plestil, J. and Baldrian, J. *Makromol. Chem.* 1975, **176**, 1009
23 Hilfiker, R., Chu, B. and Xu, Z. *J. Colloid Interface Sci.* 1989, **133**, 176
24 Mortensen, K. and Brown, W. *Macromolecules* 1993, **26**, 4128
25 Yang, L., Bedells, A. D., Attwood, D. and Booth, C. *J. Chem. Soc., Faraday Trans.* 1992, **88**, 1447
26 Biggs, S. and Vincent, B. *Colloid Polym. Sci.* 1992, **270**, 511
27 Yu, G.-E., Deng, Y., Dalton, S., Wang, Q.-G., Attwood, D., Price, C. and Booth, C. *J. Chem. Soc., Faraday Trans.* 1992, **88**, 2537
28 Malmstem, M. and Lindman, B. *Macromolecules* 1992, **25**, 5434
29 Tuzar, Z., Petrus, V. and Kratochvil, P. *Makromol. Chem.* 1974, **175**, 3181
30 Hirao, A., Yamamoto, A., Takenaka, K., Yamaguchi, K. and Nakahama, S. *Polymer* 1987, **28**, 303
31 Pike, E. R., Pomeroy, W. R. M. and Vaughan, J. M. *J. Chem. Phys.* 1975, **62**, 3188
32 Koppel, D. E. *J. Chem. Phys.* 1972, **57**, 4814
33 Zimm, B. H. and Stockmayer, W. H. *J. Chem. Phys.* 1949, **17**, 1301
34 Miyake, A. and Freed, K. F. *Macromolecules* 1983, **16**, 1228
35 Douglas, J. F. and Freed, K. F. *Macromolecules* 1984, **17**, 2344
36 Douglas, J. F., Roovers, J. and Freed, K. F. *Macromolecules* 1990, **23**, 4168
37 Roovers, J. E. L., Toporowski, P. and Martin, J. *Macromolecules* 1989, **22**, 1897
38 Takano, A., Okada, M. and Nose, T. *Polymer* 1992, **33**, 783
39 Kato, T., Miyaso, K., Noda, I., Fujimoto, T. and Nagasawa, M. *Macromolecules* 1970, **3**, 777
40 Vegberg, L. J. M., Cogan, K. A. and Gast, A. P. *Macromolecules* 1991, **21**, 1670
41 Lin, J.-L. and Roe, R.-J. *Macromolecules* 1987, **20**, 2168
42 Miyaki, Y., Einaga, Y. and Fujita, H. *Macromolecules* 1978, **11**, 1180
43 Tanaka, G., Imai, S. and Yamakawa, H. *J. Chem. Phys.* 1970, **52**, 2639
44 Lang, J., Tondre, C., Zana, R., Bauer, R., Hoffmann, H. and Ulbricht, W. *J. Phys. Chem.* 1975, **79**, 276
45 Sikora, A. and Karaz, F. E. *Macromolecules* 1993, **26**, 177
46 Benoit, H. and Frolich, D. in 'Light Scattering from Polymer Solutions' (Ed. M. B. Huglin), Academic Press, London, 1972, Ch. 11
47 Burchard, W. *Adv. Polym. Sci.* 1983, **48**, 53
48 Kinning, D. J., Thomas, E. L. and Fetters, L. J. *Macromolecules* 1991, **24**, 3893

APPENDIX 1

Calculation for radii of gyration of spherical micelles measured by scattering experiments

Consider a spherical micelle that has a scattering ability $w(x)$ given as a function of the reduced distance x from the centre of the micelle. The variable x is defined as $x = r/R$, with r being the distance from the centre and R the outer radius of the micelle. The function $w(x)$ is the product of the polymer concentration $c(x)$ within the micelle and the specific scattering ability $n(x)$ of the polymer, i.e. $w(x) = c(x)n(x)$. Here $c(x)$ is expressed in mass/(solution volume) and $n(x)$ corresponds to the refractive-index increment for increase of unit polymer concentration. Then, the measured apparent radius of gyration R_g is expressed as[46,47]:

$$R_g^2 = \frac{\int\int n(\mathbf{r}_1)c(\mathbf{r}_1)n(\mathbf{r}_2)c(\mathbf{r}_2)(\mathbf{r}_1 - \mathbf{r}_2)^2 \, d\mathbf{r}}{2\left(\int n(\mathbf{r})c(\mathbf{r}) \, d\mathbf{r}\right)^2} = \frac{R^2 \int_0^1 x^4 w(x) \, dx}{\int_0^1 x^2 w(x) \, dx} \tag{7}$$

The total polymer mass M of the micelle is given by:

$$M = 4\pi R^3 \int_0^1 x^2 c(x) \, dx \tag{8}$$

To know the micelle structure is to determine the profile $c(x)$. In the following, we present models for $c(x)$ and how it can be determined from experimental quantities. Here, we make an assumption that the outer radius R is equal to R_h, since the segment density in the micelle is considered to be sufficiently high to assume non-draining owing to the hydrodynamic interactions between segments in the micelle.

Three models are considered for the micelle structure as in the following (see *Figure 10*):

(a) A core–corona with uniform segment density (*Figure 10a*). The profile $c(x)$ is given as:

$$c(x) = \begin{cases} c_i & 0 < x < x_i \\ c_s & x_i < x < 1 \end{cases}$$

$$n(x) = \begin{cases} n_i & 0 < x < x_i \\ 0 & x_i < x < 1 \end{cases}$$

(b) A core–corona with segment-density gradient (*Figure 10b*). The profile $c(x)$ is approximated by the following equation:

$$c(x) = \begin{cases} d_i & 0 < x < x_0 \\ d_i + (x - x_0)(d_i - c_s)/(x_0 - x_i) & x_0 < x < x_i \\ c_s & x_i < x < 1 \end{cases}$$

$$n(x) = \begin{cases} n_i & 0 < x < x_i \\ 0 & x_i < x < 1 \end{cases}$$

(d_i = density of the core polymer).

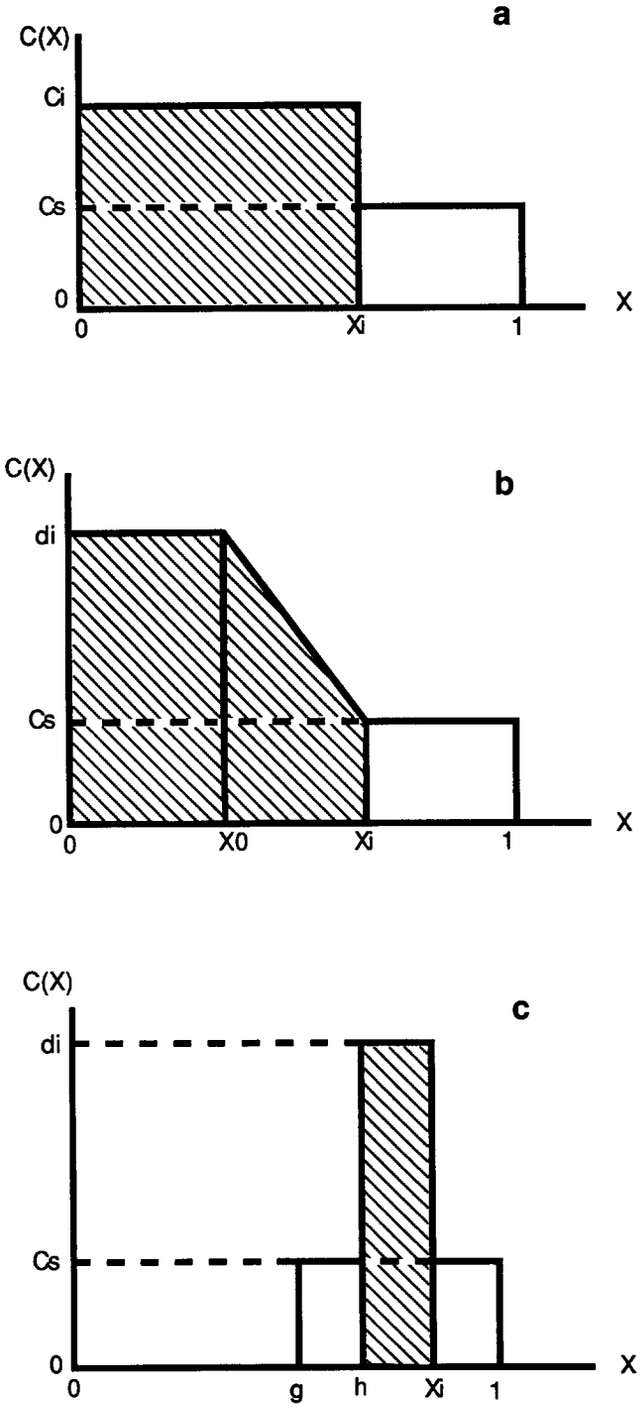

Figure 10 Definition of polymer-concentration profile in a micelle for three models: (a) a core–corona with uniform segment density; (b) a core–corona with segment-density gradient; and (c) a vesicle. Shaded areas represent segregated core parts of micelles

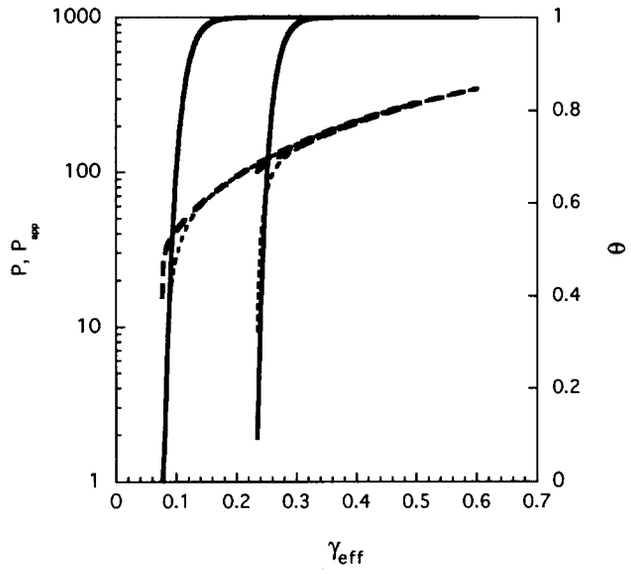

Figure 11 Calculated curves for P and θ against γ_{eff} for $N_0 = 700 > N_1 = 100$ at concentrations $\phi = 10^{-6}$ and 10^{-10} in polymer volume fraction: association number P (▬▬); apparent association number P_{app} (-----); micelle fraction θ (▬▬)

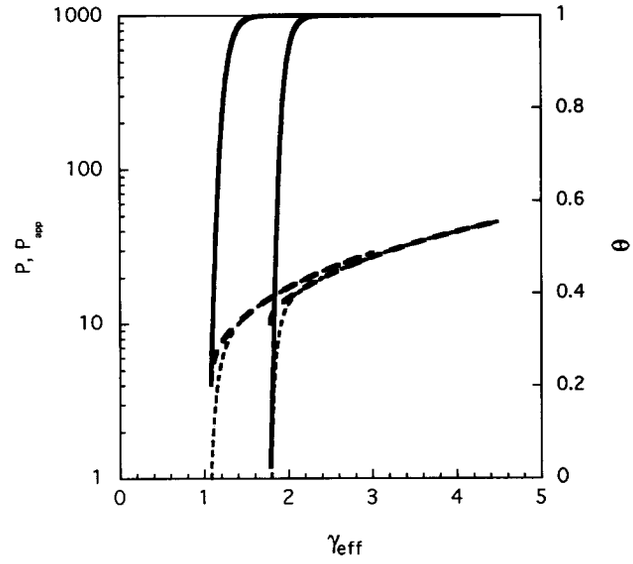

Figure 12 Calculated curves for P and θ against γ_{eff} for $N_0 = 100 < N_1 = 700$ at concentrations $\phi = 10^{-6}$ and 10^{-10} in polymer volume fraction: association number P (▬▬); apparent association number P_{app} (-----); micelle fraction θ (▬▬)

(c) A vesicle (*Figure 10c*). The profile $c(x)$ is given as:

$$c(x) = \begin{cases} 0 & 0 < x < g \\ c_s & g < x < h \text{ with } h - g = 1 - x_i \\ d_i & h < x < x_i \\ c_s & x_i < x < 1 \end{cases}$$

$$n(x) = \begin{cases} n_i & h < x < x_i \\ 0 & g < x < h \text{ and } x_i < x < 1 \end{cases}$$

The polymer mass M_i of the core is given for (a) and (b) by:

$$M_i = 4\pi R^3 \int_0^{x_i} x^2 c(x)\, dx \qquad (9)$$

For the vesicle (c), one has:

$$M_i = 4\pi R^3 \int_h^{x_i} x^2 c(x)\,dx \tag{10}$$

What we can obtain experimentally are R_g, R_h, M, M_i and d, and we can approximate R by R_h.

If R_g/R, $M/4\pi R^3$ and M_i/M are given, then equations (7), (8) and (9) or (10) can determine the profile characterized by the three parameters with d_i for each case: x_i, c_i and c_s for (a); x_0, x_i and c_s for (b); and h, x_i and c_s for (c). The density d_i of PαMS was put at 1.1296 g cm^{-3} (ref. 41). The effect of the non-zero dn/dC of PVPA blocks was calculated on the basis of equation (7) to be less than 0.7% in terms of R_g. This is small enough and the approximation of $n(x) = 0$ for PVPA blocks in the above models is acceptable for the present purpose.

APPENDIX 2

Calculations of association number and micelle-forming fraction of polymers near cmc *based on the LOW theory*

We suppose a dilute solution of diblock copolymers consisting of A and B blocks with the polymeric indices being N_0 and N_1, respectively, in a selective solvent. The block copolymers form core–corona type micelles with non-swollen core of A blocks and corona of B blocks. Here, a two-state model is adopted, that is, the micelles have monodisperse association number. Consequently, letting the volume fraction of micelle-forming polymers be denoted by θ, then $(1-\theta)$ is the volume fraction of unimers in the total polymers. Therefore, the numbers of micelles and unimers per site are $\theta\phi/PN$ and $(1-\theta)\phi/N$, respectively, where N is the total polymeric index $N_0 + N_1$, P is the association number and ϕ is the volume fraction of the total copolymer in the solution. Then, the free energy $kT\Delta f$ of the whole system per site is given, in the framework of the Flory–Huggins type theory, by:

$$\Delta f = (\theta\phi/PN)\ln(\theta\phi) + [(1-\theta)\phi/N]\ln[(1-\theta)\phi] + (1-\phi)\ln(1-\phi) + \theta\phi F_m/PN + \phi(1-\theta)F_u/N \tag{11}$$

Here, kTF_m and kTF_u are the free energies of a micelle and a unimer, respectively, with k being the Boltzmann constant and T the absolute temperature. Following calculations of the LOW theory[2,7], F_m is given as the sum of free energies of interface, corona and core, i.e.:

$$F_m = F(\text{interface}) + F(\text{corona}) + F(\text{core}) \tag{12}$$

with

$$F(\text{interface}) = \gamma_{\text{eff}} N_0^{2/3} P^{2/3} \tag{13}$$

$$F(\text{corona}) = P^{3/2}\ln(N_0^{-1/3}P^{-2/15}N_1^{3/5}) \tag{14}$$

and

$$F(\text{core}) = \tfrac{3}{2}P(AP^{2/3}N_0^{-1/3} + A^{-1}P^{-2/3}N_0^{1/3} - 2) \tag{15}$$

Here, $kT\gamma_{\text{eff}}$ is an effective free energy of interface between the core and the corona, which changes with solvent quality. The term $F(\text{core})$ comes from the elastic free energy of chain deformation in the core with $A = (4\pi/3)^{-2/3}$ in a rough approximation, and here A is regarded as an appropriate constant of the order of unity.

Self-consistency of the theory demands that $F_u = F_m(P = 1)$, which leads to:

$$F_u = \gamma_{\text{eff}} N_0^{2/3} + \ln(N_0^{-1/3}N_1^{3/5}) + \tfrac{3}{2}(AN_0^{-1/3} + A^{-1}N_0^{1/3} - 2) \tag{16}$$

Substituting equations (12)–(16) into (11), one has the expression of Δf as a function of θ, P, γ_{eff} and ϕ for a given set of N_0 and N_1.

In the equilibrium state, parameters θ and P follow the equilibrium conditions:

$$\partial\Delta f/\partial\theta = 0 \tag{17}$$

$$\partial\Delta f/\partial P = 0 \tag{18}$$

These two equations yield the following simultaneous equations that determine θ and P in equilibrium as functions of ϕ and γ_{eff} for given values of N_0 and N_1:

$$\ln(\theta\phi) + \gamma_{\text{eff}}N_0^{2/3}P^{2/3}/3 - P^{3/2}[\tfrac{1}{2}\ln(N_0^{-1/3}P^{-2/15}N_1^{3/5}) - \tfrac{2}{15}] - AP^{5/3}N_0^{-1/3} + A^{-1}P^{1/3}N_0^{1/3} = 0 \tag{19}$$

$$2\ln(\theta\phi)/P - 1/P + \ln[\phi(1-\theta)] + 1 + \gamma_{\text{eff}}N_0^{2/3} + \ln(N_0^{-1/3}N_1^{3/5}) - P^{1/2}[\tfrac{5}{2}\ln(N_0^{-1/3}P^{-2/15}N_1^{3/5}) - \tfrac{2}{5}] + \tfrac{3}{2}(AN_0^{-1/3} + A^{-1}N_0^{1/3}) - \tfrac{9}{2}AP^{2/3}N_0^{-1/3} + \tfrac{3}{2}A^{-1}P^{-2/3}N_0^{1/3} = 0 \tag{20}$$

Changes of P and θ with γ_{eff} were calculated for sets ($N_0 = 700$, $N_1 = 100$) and ($N_0 = 100$, $N_1 = 700$) shown in *Figures 11* and *12*, respectively. Here, A was put to be 1.2. Expected apparent association number P_{app} measured by light scattering, which is given by $P_{\text{app}} = P\theta$, is also plotted in the figures. It should be noted that this type of theory generally underestimates the *cmc* (see ref. 48, for instance). It is noteworthy that the association number P of micelles for $N_0 > N_1$ is larger than that for $N_0 < N_1$. This is consistent with the experimental result that P_{app} in CBA-rich solvents is larger than that in CBC-rich solvents. A micelle of $N_0 < N_1$ needs strong segregation, i.e. large γ_{eff}, while weak segregation of small γ_{eff} can make a micelle of $N_0 > N_1$.